Photoinduced magnetic bound state in an itinerant correlated electron system with a spin-state degree of freedom

Yu Kanamori,[1] Jun Ohara,[1,2,*] and Sumio Ishihara[1,2]
[1]*Department of Physics, Tohoku University, Sendai 980-8578, Japan*
[2]*Core Research for Evolutional Science and Technology (CREST), Sendai 980-8578, Japan*
(Received 9 April 2012; published 30 July 2012)

The photoexcited state in a correlated electron system with a spin-state degree of freedom is studied. We start from the two-orbital extended Hubbard model where the energy difference between the two orbitals is introduced. The photoexcited metastable state is examined based on the effective model Hamiltonian derived using the two-orbital Hubbard model. Spin-state change is induced by photoirradiation in the low-spin band insulator near the phase boundary, and it is found that a high-spin state is stabilized by creating a ferromagnetic bound state with photodoped hole carriers. An optical absorption occurs between the bonding and antibonding orbitals inside the bound state. The time evolution of photoexcited states is simulated in the time-dependent mean-field scheme. It is found that pair annihilations of photodoped electrons and holes generate the high-spin state in a low-spin band insulator. We propose that this process is directly observed by the time-resolved photoemission experiments.

DOI: 10.1103/PhysRevB.86.045137 PACS number(s): 78.20.Ls, 71.10.−w, 78.20.Bh, 78.47.J−

I. INTRODUCTION

The optical properties and photoinduced phenomena in solids are subjects of considerable interest in recent solid-state physics studies. In particular, correlated electron systems are the principal subject for the investigation of photoinduced exotic phenomena. These systems exhibit strong electron-electron interaction and multiple degrees of freedom, e.g., spin, charge, and orbital, and consequently numerous electronic and structural phases are realized under a subtle balance of interactions.[1] By irradiating intense laser pulses into one of the phases, a system can be transferred into a different phase transiently or permanently. This is termed photoinduced phase transition (PIPT).[2] Several experimental and theoretical studies have been made on PIPT phenomena in transition-metal oxides,[3–7] low-dimensional organic salts,[8–11] and other materials.

Among the various degrees of freedom, the spin-state degree of freedom has attracted much attention from the viewpoint of the optical manipulation of magnetism. In certain magnetic ions, a different magnitude of spin angular momentum is realized by changing external fields, such as temperature, pressure, and photons. This is termed the spin-state transition and is caused by a competition between the crystal-field splitting and the Hund's rule coupling. A well-known example of a photoinduced spin-state change is seen in the so-called spin-crossover complexes, such as the Prussian blue analog complex.[12–15] Here, photons cause a charge transfer from the Fe ions to Co ions, associated with the spin-state change in the Co ions from the low-spin (LS) state to the high-spin (HS) state. The main mechanism of the cooperative spin-state transition in the series of materials is believed to be an elastic interaction[16–19] where a local volume change of a metal-ligand cluster propagates over a crystal lattice.

Another material where photoinduced spin-state change is realized is the perovskite cobaltites $R_{1-x}A_xCoO_3$ (R: rare-earth ion, A: alkaline-earth ion) and their families.[20–22] In an undoped compound $LaCoO_3$,[23,24] the formal valence of the Co ion is 3+ with a d^6 electron configuration. There are three possible spin states: the LS state with the $(t_{2g})^6(e_g)^0$ configuration, the intermediate-spin (IS) state with $(t_{2g})^5(e_g)^1$, and the HS state with $(t_{2g})^4(e_g)^2$. It is inferred from electric resistivity and magnetic susceptibility measurements that the LS band insulator at low temperatures changes into the HS or IS metallic state with increasing temperature (T).[25–28] By substituting R with A, corresponding to hole doping into the nonmagnetic insulating ground state, the system shows ferromagnetic metallic behavior.[29–32] One key point for understanding the electronic and magnetic properties in cobaltites is the strong correlation between electron conduction and magnetism, i.e., the charge and spin degrees of freedom of the electrons.[33]

The optical irradiation and manipulation of perovskite cobaltites and related materials have been examined by ultrafast optical pump-probe measurements.[34,35] Recently, detailed experiments and analyses have been made in so-called A-site ordered perovskite-type $RBaCo_2O_{6-\delta}$ crystals by Okimoto and co-workers.[34] After pump pulse is introduced into the LS insulator, a metallic state, which is different from the high-temperature metallic state, is observed in the optical conductivity spectra. This photoinduced state strongly depends on the R species, which is believed to control the ratio of electron correlation and bandwidth. These experiments suggest that strong correlation between the electronic and magnetic states remains even in the photoexcited state, and indicate that the photoirradiation phenomena in the cobalt oxides should be reexamined from a different viewpoint from the photoinduced spin-state change in spin-crossover complexes.

In this paper, photoinduced spin-state change in correlated electron systems is studied theoretically. From the two-orbital Hubbard model, the effective Hamiltonian for the photoexcited state is derived. The photoexcited metastable state is obtained through an analysis of the effective Hamiltonian using the exact-diagonalization method. By the irradiation of photons into the LS band insulator near the phase boundary, the HS state

is induced. It is found that the HS state is stabilized by forming a bound state with a photodoped hole. This bound state causes a characteristic peak structure in the optical spectra in the photoexcited state. The time evolution after photoirradiation is examined in the time-dependent mean-field scheme. The HS state is created by pair annihilation of photodoped electron and hole. This mechanism can be confirmed by time-resolved photoemission spectroscopy experiments.

In Sec. II, the model Hamiltonian and the effective model for the photoexcited states are introduced. In Sec. III, numerical results of the electronic states before and after photoirradiation are presented. In Sec. IV, the time dependence of the photoexcited states is shown. Section V is devoted to discussion and concluding remarks. A brief report on previous studies of the photoinduced metastable state was published in Ref. 36.

II. MODEL

A. Two-orbital Hubbard model

We start with the two-orbital Hubbard model as a minimal model to examine photoinduced spin-state change. Two orbitals, termed A and B corresponding to the e_g and t_{2g} orbitals in a Co ion, respectively, are introduced at each site in a lattice. The crystal-field splitting between A and B is represented by $\Delta = \varepsilon_A - \varepsilon_B > 0$ where ε_A and ε_B are the level energies of the A and B orbitals, respectively. The model Hamiltonian is given as

$$\mathcal{H} = \mathcal{H}_U + \mathcal{H}_t, \tag{1}$$

where we define the on-site term,

$$\mathcal{H}_U = \Delta \sum_{i\sigma} c^\dagger_{iA\sigma} c_{iA\sigma} + U \sum_{i\gamma} n_{i\gamma\uparrow} n_{i\gamma\downarrow} + U' \sum_{i\sigma\sigma'} n_{iA\sigma} n_{iB\sigma'} + J \sum_{i\sigma\sigma'} c^\dagger_{iA\sigma} c^\dagger_{iB\sigma'} c_{iA\sigma'} c_{iB\sigma} + I \sum_{i\gamma} c^\dagger_{i\gamma\uparrow} c^\dagger_{i\gamma\downarrow} c_{i\bar{\gamma}\downarrow} c_{i\bar{\gamma}\uparrow}, \tag{2}$$

and the intersite term,

$$\mathcal{H}_t = -\sum_{\langle ij\rangle\gamma\sigma} t_\gamma (c^\dagger_{i\gamma\sigma} c_{j\gamma\sigma} + \text{H.c.}). \tag{3}$$

Here, $c^\dagger_{i\gamma\sigma}$ is the electron creation operator at site i with orbital γ (=A, B) and spin σ (=↑,↓). We define the number operator $n_{i\gamma\sigma} = c^\dagger_{i\gamma\sigma} c_{i\gamma\sigma}$ and subscript $\bar{\gamma}$ = (A, B) for γ = (B, A). The intraorbital Coulomb interaction U, interorbital Coulomb interaction U', pair-hopping I, and Hund's rule coupling J are introduced. The electron transfer integrals between the nearest-neighboring (NN) sites are set to be diagonal with respect to the orbital. We assume a relation $t_B < t_A$ by considering the transfer integrals in perovskite oxides, and we take $t_A = 1$ as the unit of energy.

Let us consider the local electronic structure, in which two electrons occupy each site, and the electron transfers are set to be zero. The following $S = 0$ and $S = 1$ states are the two possible ground states [see Figs. 1(a) and 1(b)]. The eigenfunction and eigenenergy for the LS state are given as

$$|\psi_L\rangle = (f_A c^\dagger_{A\uparrow} c^\dagger_{A\downarrow} + f_B c^\dagger_{B\uparrow} c^\dagger_{B\downarrow})|0\rangle \tag{4}$$

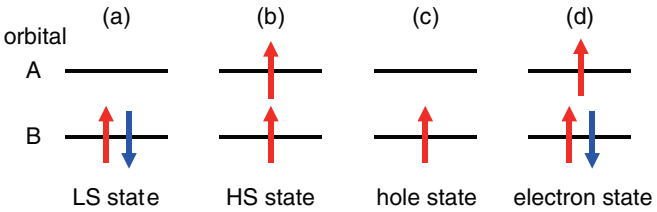

FIG. 1. (Color online) Local electronic configurations.

and $E_L = U + \Delta - \sqrt{\Delta^2 + I^2}$, respectively, with the coefficients

$$f_B = \left[1 + \left(\frac{\Delta}{I} - \sqrt{1 + \frac{\Delta^2}{I^2}}\right)^2\right]^{-1/2} \tag{5}$$

and

$$f_A = \sqrt{1 - f_B^2}. \tag{6}$$

The wave functions for the HS state are given by

$$|\psi_{H+1}\rangle = c^\dagger_{A\uparrow} c^\dagger_{B\uparrow} |0\rangle, \tag{7}$$

$$|\psi_{H0}\rangle = \frac{1}{\sqrt{2}}(c^\dagger_{A\uparrow} c^\dagger_{B\downarrow} + c^\dagger_{A\downarrow} c^\dagger_{B\uparrow})|0\rangle, \tag{8}$$

$$|\psi_{H-1}\rangle = c^\dagger_{A\downarrow} c^\dagger_{B\downarrow} |0\rangle, \tag{9}$$

for $S^z = +1$, 0, and -1, respectively, and the energy in the HS triplet state is $E_H = U' + \Delta - J$. These states are termed the LS and HS states in the present two-orbital Hubbard model, although the HS state takes $S = 2$ in a Co^{3+} ion in cobaltites. In the numerical simulations, for simplicity, we assume the relations $U - U' = 2J$, $U = 4J$, and $I = J$, to reduce the number of free parameters. We confirm that the qualitative results are robust for a wide parameter region. The LS and HS states are degenerate at $\Delta = J/\sqrt{3}$. We do not fix the parameter values for cobaltites, but calculate the electronic structures for a wide parameter range, since several simplifications are introduced in the model Hamiltonian to avoid complications in real materials.

B. Effective Hamiltonian

One of the main purposes of this paper is to examine a stable steady photoexcited state, defined as the lowest energy state inside an energy surface, where the density of the photoexcited electron-hole pairs is fixed. A schematic picture of this state is shown in Fig. 2. The bold curves represent the adiabatic energy surfaces before and after photoirradiation as functions of the number of HS sites. Photons excite the system from the lowest energy surface to a higher energy surface. Through several kinds of relaxation processes, the system settles to the lowest energy state in the higher energy surface. Instead of performing time-dependent simulations for the photoexcited dynamics, we examine the lowest energy state inside the energy surface where there is one electron-hole pair in an N-site system. This state is termed the photoinduced metastable state. Finally, the system is fully relaxed from the metastable state to the initial state through several relaxation processes, although simulations for these processes are beyond the present study. We derive the two effective Hamiltonians, where the numbers

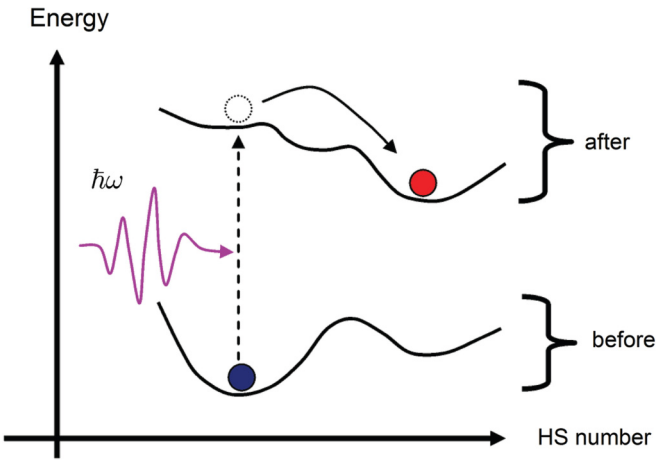

FIG. 2. (Color online) Adiabatic energy surfaces before and after photoirradiation. Horizontal axis represents the number of the HS state.

of electron-hole pairs are zero and one in an N-site system, and obtain the initial and metastable states by analyzing the lowest energy states in the two Hamiltonians.

The effective Hamiltonians are derived by perturbational processes from the two-orbital Hubbard model in Eq. (1). The intersite transfer term $\mathcal{H}_t$ is treated as the perturbation term. As for the effective Hamiltonian before the photoirradiation, the HS and LS states, defined in Eq. (4) and Eqs. (7)–(9), respectively, are adopted as the basis states. Other local states, where two electrons occupy each site, have higher energies of the order of Δ, J, and U than the LS and HS sates. By considering all the second-order perturbational processes, the Hamiltonian is given as

$$\begin{aligned}\mathcal{H}_0 = \mathcal{H}_U &+ J_{HH}\sum_{\langle ij\rangle}(\boldsymbol{S}_i\cdot\boldsymbol{S}_j-1)P_i^HP_j^H\\ &- J_{LL}\sum_{\langle ij\rangle}P_i^LP_j^L - J_{HL}\sum_{\langle ij\rangle}\left(P_i^LP_j^H+P_i^HP_j^L\right)\\ &- J_{++}\sum_{\langle ij\rangle}[I_i^-I_j^-(\boldsymbol{S}_i\cdot\boldsymbol{S}_j-1)+(\boldsymbol{S}_i\cdot\boldsymbol{S}_j-1)I_i^+I_j^+]\\ &+ J_{+-}\sum_{\langle ij\rangle}[I_j^-(\boldsymbol{S}_i\cdot\boldsymbol{S}_j+1)I_i^+ + I_i^-(\boldsymbol{S}_i\cdot\boldsymbol{S}_j+1)I_j^+].\end{aligned} \tag{10}$$

Here, $\boldsymbol{S}_i$ is the spin operator defined by $\boldsymbol{S}_i = (1/2)\sum_{\gamma\sigma\sigma'}c_{i\gamma\sigma}^\dagger\boldsymbol{\sigma}_{\sigma\sigma'}c_{i\gamma\sigma'}$ with the Pauli matrices $\boldsymbol{\sigma}$, and P_i^L and P_i^H are the projection operators for the LS and HS state defined by

$$P_i^L = |\psi_{Li}\rangle\langle\psi_{Li}| \tag{11}$$

and

$$P_i^H = \sum_{l=(+,0,-)}|\psi_{Hli}\rangle\langle\psi_{Hli}|, \tag{12}$$

respectively. The operators I_i^+ and I_i^- change the spin state as

$$I_i^+ = |\psi_{H0i}\rangle\langle\psi_{Li}| \tag{13}$$

and

$$I_i^- = |\psi_{Li}\rangle\langle\psi_{H0i}|. \tag{14}$$

The prefactors in each term in Eq. (10) are the exchange constants and their explicit forms are presented in Appendix A.

The effective Hamiltonian after photoirradiation is derived in the same way. As the unperturbed states, in addition to the LS and HS states, we introduce the states where the number of electrons in a site is one or three [see Figs. 1(c) and 1(d)]. These local states are termed the hole state and the electron state, respectively. The wave functions are given as

$$|\psi_{h\sigma}\rangle = c_{A\sigma}^\dagger|0\rangle \tag{15}$$

and

$$|\psi_{e\sigma}\rangle = c_{A\sigma}^\dagger c_{B\uparrow}^\dagger c_{B\downarrow}^\dagger|0\rangle, \tag{16}$$

respectively. The eigenenergies are $E_e = \Delta + U + 2U' - J$ for the electron state and $E_h = 0$ for the hole state. We assume that the number of both the electron state and the hole state is one in an N-site cluster. The calculated effective Hamiltonian is classified by the electronic states in the NN sites as

$$\mathcal{H}_1 = \widetilde{\mathcal{H}}_0 + \mathcal{H}_{eh} + \mathcal{H}_e + \mathcal{H}_h. \tag{17}$$

The first term $\widetilde{\mathcal{H}}_0$ corresponds to $\mathcal{H}_0$ in Eq. (10), where neither the electron or hole state is involved in the interactions. The second term applies for the interactions between the electron state and the hole state. The third and fourth terms describe the interactions between the electron state and LS or HS, and the interactions between the hole state and LS or HS, respectively. Explicit forms for the Hamiltonian are given in Appendix B.

The ground state before photoirradiation and the photoinduced metastable state are obtained with the effective Hamiltonians in Eqs. (10) and (17), respectively, which are analyzed by the exact-diagonalization method based on the Lanczos algorithm. The time evolutions in the photoinduced dynamics are calculated in the two-orbital Hubbard model in Eq. (1).

III. ELECTRONIC STATES BEFORE AND AFTER PHOTOIRRADIATION

A. Ground state

The electronic structure in the ground state is examined by analyzing the effective Hamiltonian $\mathcal{H}_0$ in a finite size cluster system. Several physical quantities are plotted in Fig. 3 as a function of the Hund's rule coupling J at $\Delta/t_A = 10$. We introduce the number density of the HS states which is estimated from the electron number in the orbital A defined by

$$n_{HS} = \frac{1}{N}\sum_i\langle n_{iA}\rangle, \tag{18}$$

the spin correlation function,

$$S(\boldsymbol{q}) = \frac{1}{2N^2}\sum_{ij}e^{-i\boldsymbol{q}\cdot(\boldsymbol{r}_i-\boldsymbol{r}_j)}\langle\boldsymbol{S}_i\cdot\boldsymbol{S}_j\rangle, \tag{19}$$

and the spin-state correlation function defined by

$$I(\boldsymbol{q}) = \frac{4}{N^2}\sum_{ij}e^{-i\boldsymbol{q}\cdot(\boldsymbol{r}_i-\boldsymbol{r}_j)}\langle I_i^zI_j^z\rangle. \tag{20}$$

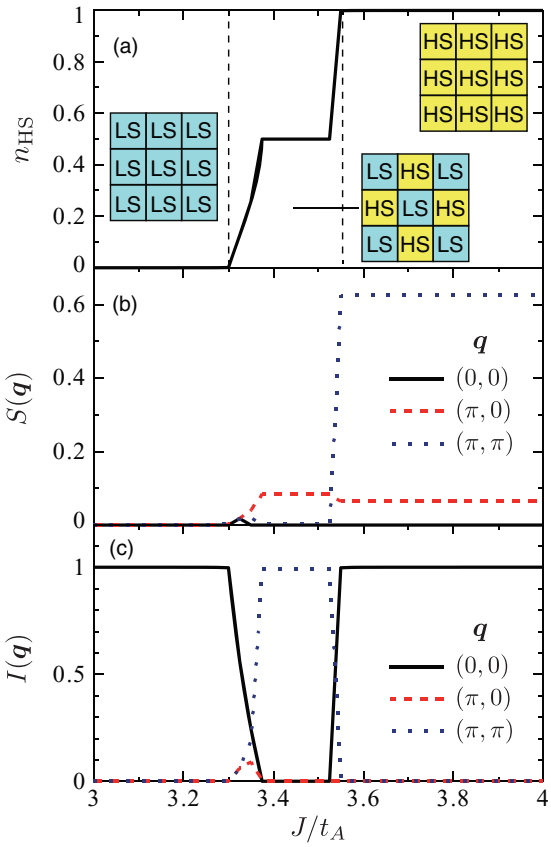

FIG. 3. (Color online) (a) The number density of the HS state $n_{\rm HS}$, (b) the spin correlation function $S(\boldsymbol{q})$, and (c) the spin-state correlation function $I(\boldsymbol{q})$ in the ground state. The parameters are chosen to be $U = 4J$, $U' = 2J$, $\Delta = 10t_A$, and $t_B = 0.05t_A$. A two-dimensional cluster of the $N = 8$ sites with the periodic boundary condition is adopted.

Here, we define the spin-state operator as a projection operator by

$$I_i^z = \frac{1}{2}\sum_{m=\pm1,0}(|\psi_{Hmi}\rangle\langle\psi_{Hmi}| - |\psi_{Li}\rangle\langle\psi_{Li}|), \qquad (21)$$

which takes $1/2$ and $-1/2$ for the HS and LS states, respectively. With increasing J, three different phases appear in Fig. 3. In the region of small J, both $n_{\rm HS}$ and $S(\boldsymbol{q})$ are zero, and $I(0,0)$ is almost one. On the other hand, in the region of large J, $n_{\rm HS}$ and $I(0,0)$ are one, and $S(\pi,\pi)$ takes its largest value. Two phases are identified as the LS band insulator and the HS antiferromagnetic Mott insulator. Between the two, there is an intermediate phase where $n_{\rm HS} = 0.5$, and $I(\pi,\pi)$ is one. These data imply that the HS and LS states are aligned alternately. This phase is termed the spin-state ordered phase.[37] This alternate ordering of the HS and LS states is caused by the fourth term on the right-hand side in Eq. (10); J_{HL} given in Eq. (A3) represents the attractive interaction between the LS and HS states.

The numerical data for several J and Δ are summarized in the phase diagram shown in Fig. 4, where the phase boundaries in the ground state and those in the photoinduced metastable state are plotted in one figure. The detailed results

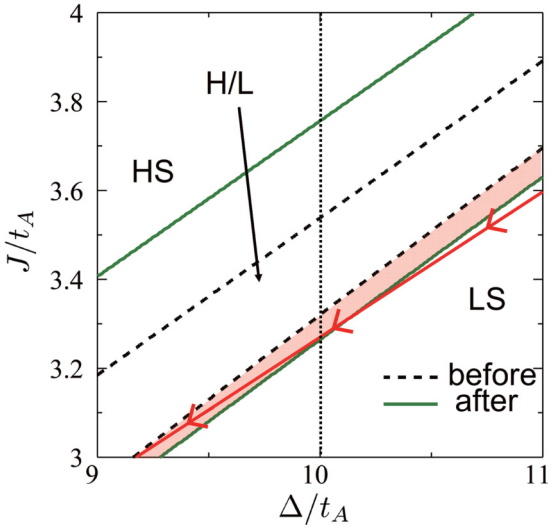

FIG. 4. (Color online) Phase diagram in the plane of the crystal-field splitting Δ and the Hund's rule coupling J. The broken and bold lines represent the phase boundaries in the ground state and in the photoinduced metastable state, respectively. The abbreviations HS, LS, and H/L represent the HS phase, the LS phase, and the HS-LS mixed phase, respectively. The vertical dotted line represents the parameter region where the data in Figs. 3 and 5 are calculated. The parameters are chosen to be $U = 4J$, $U' = 2J$, and $t_B = 0.05t_A$. A two-dimensional cluster of the $N = 8$ sites with a periodic boundary condition is adopted.

in the metastable state will be presented in Sec. III B. Here, we identify the LS and HS phases as states, where the electron numbers of the A orbital are smaller or larger than 0.3, respectively. We confirm that the size dependence of the phase boundaries is of the order of $0.01t_A$. It is observed that the LS and HS phases are stabilized in regions of large Δ and large J, respectively, and the spin-state ordered phase denoted by H/L appears between the two phases.

B. Photoinduced metastable state

Several physical quantities in the photoinduced metastable state are presented in Fig. 5 as a function of the Hund's rule coupling J at $\Delta/t_A = 10$. The number density of HS states is estimated from the number of electrons in the orbital A defined by

$$n_{\rm HS} = \frac{1}{N-2}\left(\sum_i \langle n_{iA}\rangle - 1\right), \qquad (22)$$

where the electron and hole states are subtracted in the denominator. It is shown in Fig. 5(a) that $n_{\rm HS}$ in the photoinduced metastable state is finite within $3.25 < J/t_A < 3.30$ where $n_{\rm HS} = 0$ in the ground state. The different values between the two states implies that one HS state is generated in the N-site cluster. This phase in the photoinduced metastable state is distinct from the spin-state ordered phase observed in the ground state; the spin-state correlation functions at any $\boldsymbol{q}$ are not remarkable, and a weak spin correlation at $\boldsymbol{q} = (0,0)$ is observed. Detail properties of this phase are introduced latter.

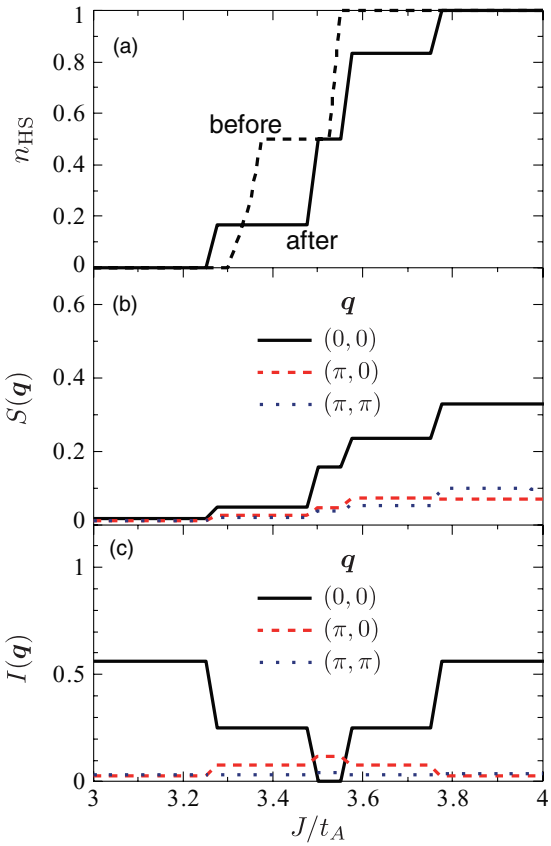

FIG. 5. (Color online) (a) Number density of the HS states $n_{\rm HS}$, (b) spin correlation function $S(\boldsymbol{q})$, and (c) spin-state correlation function $I(\boldsymbol{q})$ in the photoexcited metastable state. In comparison, results of $n_{\rm HS}$ in the ground state are also plotted in (a). The parameters are chosen to be $U = 4J$, $U' = 2J$, $\Delta = 10t_A$, and $t_B = 0.05t_A$. A two-dimensional $N = 8$ site cluster with a periodic boundary condition is adopted.

The phase diagram in the photoexcited metastable state is presented in Fig. 4, together with that in the ground state. The phase boundary between the LS and LS-HS mixed phases shifts to a region of the LS phase. There is a parameter region where the LS phase in the ground state is changed into the LS-HS mixed phase in the photoexcited metastable state. That is to say, the photoirradiation induces the HS state in the LS phase at the vicinity of the phase boundary. We note that the spin-state change also occurs from the HS phase to the mixed phase.

Now we examine the electronic structure in the photoinduced HS state in more detail. We introduce the electronic-state distribution function defined by

$$g_M(n) = z_n^{-1} \sum_{j \in nNN} \sum_i \left\langle P_{i+j}^M P_i^h \right\rangle, \tag{23}$$

where $\sum_{j \in nNN}$ implies a summation of j connecting the nth NN sites of i, and z_n is the number of the nth NN sites. The operator P_i^M $(M = L, H, e)$ is the projection operator for the M state at site i. The operators for the LS and HS states are defined in Eqs. (11) and (12), respectively, and those for the electron and hole states are defined as

$$P_i^e = \sum_\sigma |\psi_{e\sigma i}\rangle \langle \psi_{e\sigma i}| \tag{24}$$

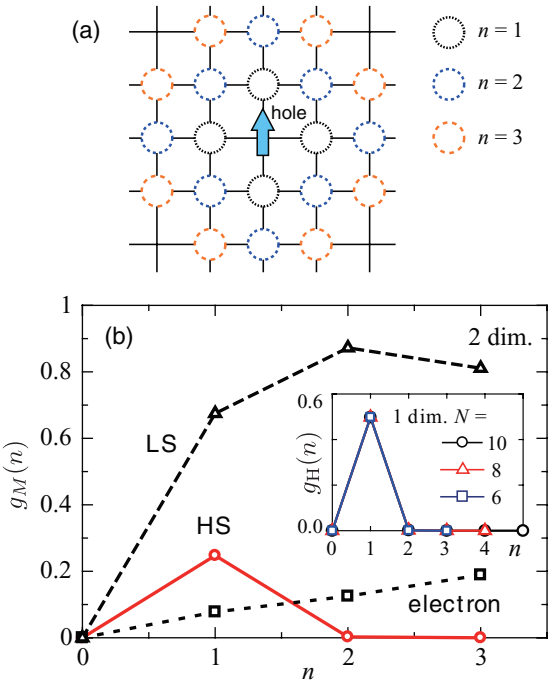

FIG. 6. (Color online) (a) Schematic definition of the distribution function $g_M(n)$. (b) Distribution function of the electronic states as a function of the distance from the hole state. The bold, broken, and dotted lines represent the distribution functions for the HS, LS, and electron states, respectively. A two-dimensional $N = 10$ site cluster with a periodic boundary condition is adopted. The inset shows distribution functions for the HS state in one-dimensional $N = 6, 8$, and 10 site clusters with a periodic boundary condition. The parameters are chosen to be $J = 3.3t_A, U = 4J, U' = 2J, \Delta = 10t_A$, and $t_B = 0.05t_A$.

and

$$P_i^h = \sum_\sigma |\psi_{h\sigma i}\rangle \langle \psi_{h\sigma i}|, \tag{25}$$

respectively. This function, $g_M(n)$, describes the distribution of the local electronic states at the nth NN sites from the photoinduced hole state, as shown in Fig. 6(a). The numerical results of the distribution functions in a two-dimensional cluster are shown in Fig. 6(b). The parameters are chosen to be $J = 3.3t_A$ and $\Delta = 10t_A$ in which the HS state is induced by photoirradiation. A characteristic feature is observed in the HS distribution function; $g_H(n)$ is nearly 0.25 at $n = 1$ and zero at $n \geqslant 2$. This implies a local bound state between the HS state and a photodoped hole state. The size dependence of $g_H(n)$ is checked in the one-dimensional clusters, and results are shown in the inset of Fig. 6(b). The HS distribution is located at the NN sites of the hole state, and almost no size dependence is seen in the results. Different numerical values of $g_H(n)$ in one- and two-dimensional clusters, i.e., 0.25 and 0.5, are attributed to a difference of z_n. The spin structure in this bound state is monitored by the correlation function defined by $\sum_{i \neq j} \langle \boldsymbol{S}_j \cdot \boldsymbol{S}_i P_j^H P_i^h \rangle$ which represents the spin correlation between the hole and HS states. The calculated value is about 0.5 which implies a ferromagnetic spin correlation. Figure 6 also shows that $g_e(n)$ monotonically increases with n. This is due to the kinetic-energy gain of the photoexcited electron. A

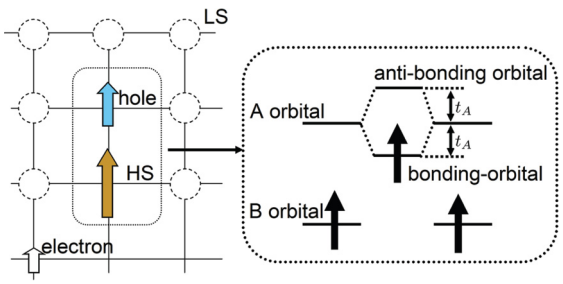

FIG. 7. (Color online) Left: Schematic picture of the HS-hole bound state. Right: Energy levels inside the HS-hole bound state.

schematic electronic structure in the photoinduced metastable state is presented in Fig. 7.

Here we discuss the mechanism of the ferromagnetic HS-hole bound state. In the ground state, the energy difference per site between the LS and HS states is given by $\Delta E_{\mathrm{HS-LS}} \equiv E_{\mathrm{HS}} - E_{\mathrm{LS}} = (U' + \Delta - J) - (U + \Delta - \sqrt{\Delta^2 + I^2})$ in the local limit. We consider the photoexcited state, where electrons and holes are introduced in the LS phase at the vicinity of the phase boundary. When the HS-hole bound state is not generated, the kinetic energy of the hole state is $-zf_B^2 t_B$ where z is the number of the NN sites, and $f_B^2 t_B$ is the exchange constant between the hole state and the LS state [see Eq. (B2)]. On the other hand, when the HS-hole bound state is generated, the energy gain is given by the bonding orbital energy in the bound state as $-t_A$ (see Fig. 7). Thus, the energy difference between the two cases is $\Delta E_{BS} = (-t_A) - (-zf_B^2 t_B)$. When this energy gain overcomes the energy cost for the HS generation, $\Delta E_{\mathrm{HS-LS}}$, the HS-hole bound state is realized.

The above consideration for the energy balance is confirmed in the bandwidth dependence of the phase diagram. In Fig. 8, the phase diagrams in the ground state and the photoinduced metastable state are plotted as functions of the ratio of the bandwidths for the A and B bands, i.e., t_B/t_A. In the region of $t_B/t_A < 0.1$, there is a phase space where the LS phase in the ground state is changed into the HS-LS mixed phase in the photoinduced metastable state. With increasing t_B/t_A, this

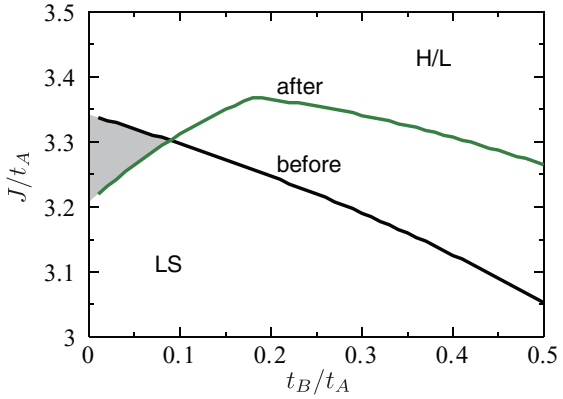

FIG. 8. (Color online) Phase diagrams in the ground state and the photoexcited metastable state in the plane of t_B/t_A and J/t_A. The shaded area shows the parameter region where the HS state is induced by photoirradiation. A two-dimensional $N = 8$ site cluster with a periodic boundary condition is adopted. The parameters are chosen to be $U = 4J$, $U' = 2J$, and $\Delta = 10t_A$.

phase space shrinks and disappears. This is explained from the above consideration where the stability of the photoinduced HS state is controlled by a factor $\Delta E_{BS} = (-t_A) - (-zf_B^2 t_B)$.

C. Optical spectra

In this subsection, we present the optical spectra in the photoinduced metastable state. The optical absorption spectra are defined by

$$\alpha^{\alpha\beta}(\omega) = -\frac{1}{N\pi}\mathrm{Im}\,\langle\psi_0|\, j^\alpha \frac{1}{\omega - \mathcal{H}^{\mathrm{eff}} + E_0 + i\eta} j^\beta\, |\psi_0\rangle\,, \tag{26}$$

where $\mathcal{H}^{\mathrm{eff}}$ is taken to be $\mathcal{H}_0$ in Eq. (10) and $\mathcal{H}_1$ in Eq. (17) for the ground state and the photoinduced metastable state, respectively, $|\psi_0\rangle$ and E_0 are the corresponding lowest energy state and energy, respectively, and α and β represent Cartesian coordinates. We introduce the current operator

$$j^\alpha = i\sum_{i\gamma\sigma} t_\gamma (c^\dagger_{i\gamma\sigma} c_{i+\alpha\gamma\sigma} - \mathrm{H.c.}), \tag{27}$$

which is defined in the restricted Hilbert space in each effective Hamiltonian. A damping constant is introduced as η. The optical spectra are calculated by the exact-diagonalization method based on the recursion procedure. Two-dimensional finite-size clusters with a periodic boundary condition are adopted.

The absorption spectra in the photoinduced metastable state, where the HS state is induced by photoirradiation, are shown in Fig. 9. The system size is taken to be $N = 8$ and 10. Two characteristic peaks appear in the spectra at $\omega = 2.1t_A$ and $\omega = 2.8t_A$ in the case of $N = 8$. These are termed the peaks B and D, and their energies are denoted ω_B and ω_D, respectively. In order to assign these peaks, we calculate the bond correlation function in the excited states given as

$$B^{(l,m)}(\omega_n) = -\sum_{\langle ij\rangle\gamma\sigma} \langle\psi(\omega_n)|\left(P_i^m P_j^l c^\dagger_{i\gamma\sigma} c_{j\gamma\sigma} P_i^l P_j^m + \mathrm{H.c.}\right)|\psi(\omega_n)\rangle, \tag{28}$$

where $|\psi(\omega_n)\rangle$ is the eigenfunction of the Hamiltonian $\mathcal{H}_1$ corresponding to the final state of the nth optical absorption peak, and ω_n is its eigenenergy. The eigenfunctions and eigenenergies are obtained by the conjugate gradient method. This function measures the bond correlation between the l and m local electronic states in the photoexcited state.

Numerical results of this correlation function together with the optical absorption spectra are presented in Fig. 9(a), where we set $(l,m) = (h,\mathrm{HS})$ and (e,LS). In the ground state, i.e., $\omega = 0$, $B^{(h,\mathrm{HS})}(\omega = 0) \sim -1$, and $B^{(e,\mathrm{LS})}(\omega = 0) \sim -3$. These values are consistent with the picture presented in Fig. 7, where a photodoped hole forms a bound state with HS, and a photodoped electron is located at the bottom of the A-orbital band. In the excited state corresponding to peak B, $B^{(e,\mathrm{LS})}(\omega_B) \simeq B^{(e,\mathrm{LS})}(0)$ and $B^{(h,\mathrm{HS})}(\omega_B) \sim 1 > B^{(h,\mathrm{HS})}(0)$. This value of $B^{(h,\mathrm{HS})}(\omega_B)$ is interpreted as indicating that an electron occupies the antibonding orbital in the HS-hole bound state, and peak B is assigned as an excitation between the bonding and antibonding orbitals inside of the bound

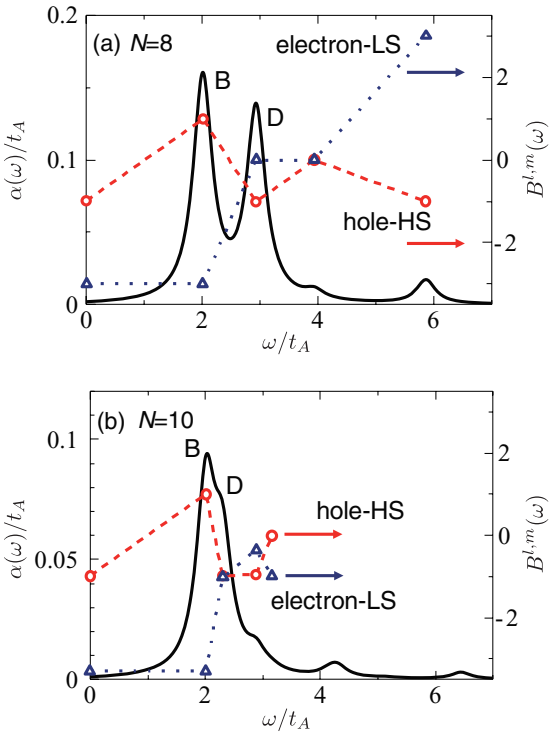

FIG. 9. (Color online) Optical absorption spectra in the photoinduced metastable state, where the HS state is induced. The bond correlation function $B^{(l,m)}(\omega)$ is also plotted. The red broken lines and blue dotted lines are for $(l,m) = (h,\mathrm{HS})$ and $(l,m) = (e,\mathrm{LS})$, respectively. The cluster size is $N = 8$ in (a) and $N = 10$ in (b). The parameters are chosen to be $J = 3.3t_A$, $U = 4J$, $U' = 2J$, $\Delta = 10.0t_A$, $t_B = 0.05t_A$, and $\eta = 0.2t_A$.

state. For peak D, $B^{(e,\mathrm{LS})}(\omega_D) > B^{(e,\mathrm{LS})}(0)$ and $B^{(h,\mathrm{HS})}(\omega_D) \simeq B^{(h,\mathrm{HS})}(0)$, which implies that a change in the photodoped electron motion is involved with this peak.

Results for clusters of size $N = 10$ are shown in Fig. 9(b). The numerical values of $B^{(h,\mathrm{HS})}$ and $B^{(e,\mathrm{LS})}$ are almost the same as those for $N = 8$. The energy of peak B is almost unchanged, but that of peak D decreases with increasing N. These size dependencies are consistent with the assignments that peak B is attributed to the local excitation, and peak D is related to the kinetic motion of the photoexcited electron. We further examine the size dependence of the peak positions in the one-dimensional clusters, and observe that the energy of peak D decreases with the system size.[36] This peak is interpreted as a Drude-like component in the thermodynamic limit.

The optical absorption spectra in the photoinduced metastable state, where HS is not induced, are presented in Fig. 10 (see bold lines). A two-peak structure is observed for $N = 10$, and the peaks almost overlap around $\omega = 3.7t_A$ for $N = 8$. The optical absorption spectra obtained in the hard-core (HC) fermion model are shown by broken lines in Fig. 10. An explicit form of the HC fermion model and a derivation are presented in Appendix C. The spectra in the effective Hamiltonian are well reproduced by the HC model. The size dependencies of the peak positions are examined in detail in this model. Two-dimensional clusters with $N = 8$, 10, 4×4, 6×6, 8×8, 10×10, 12×12 with a periodic boundary condition are adopted. The peak energies for the

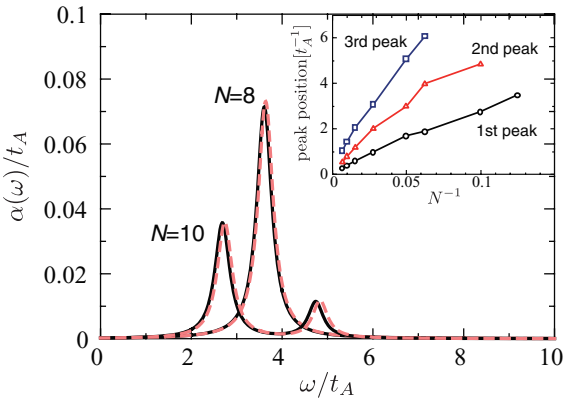

FIG. 10. (Color online) Optical absorption spectra in the photoinduced metastable state, where HS state is not induced. The broken lines represent the spectra obtained by the hard-core (HC) fermion model. The cluster sizes are $N = 8$ and 10. The inset shows the size dependencies of the peak energies in the optical absorption spectra calculated in the HC fermion model. The parameters are chosen to be $J = 3.1t_A$, $U = 4J$, $U' = 2J$, $\Delta = 10.0t_A$, $t_B = 0.05t_A$, and $\eta = 0.2t_A$ in the original model, and $t_B = 0.05t_A$, $t_{ex} = 10^{-10}t_A$, $\eta = 0.2t_A$ in the HC fermion model.

lowest three peaks are plotted in the inset of Fig. 10 as functions of N^{-1}. The energies tend to be zero in the thermodynamic limit. We interpret that these peaks originate from the metallic behaviors of photodoped electron and hole.

IV. TIME DEPENDENCE OF PHOTOEXCITED STATE

In this section, we show the real-time evolution of the photoexcited state calculated in the mean-field scheme[38,39] and reveal the mechanism of the photoinduced HS state.

A. Formulation

The time evolution of the photoexcited state is analyzed. A mean-field type decoupling is applied to the Coulomb and exchange interaction terms in the two-orbital Hubbard model in Eq. (1) as follows:

$$\begin{aligned}\mathcal{H}_{\mathrm{MF}} = \sum_{i\gamma\sigma} n_{i\gamma\sigma}\Big[U\langle n_{i\gamma\bar{\sigma}}\rangle - U'\sum_{\sigma'}\langle n_{i\bar{\gamma}\sigma'}\rangle - J\langle n_{i\bar{\gamma}\sigma}\rangle\Big] \\ - U\sum_{i\gamma}\langle n_{i\gamma\uparrow}\rangle\langle n_{i\gamma\downarrow}\rangle + U'\sum_{i\sigma\sigma'}\langle n_{iA\sigma}\rangle\langle n_{iB\sigma'}\rangle \\ + J\sum_{i\sigma}\langle n_{iA\sigma}\rangle\langle n_{iB\sigma}\rangle - \sum_{\langle ij\rangle\gamma\sigma} t_\gamma(c^\dagger_{i\gamma\sigma}c_{j\gamma\sigma} + \mathrm{H.c.}) \\ + \Delta\sum_i n_{ia}, \end{aligned} \tag{29}$$

where $\langle\cdots\rangle$ implies the average calculated by the time-dependent mean-field wave function, and the subscript $\bar{\sigma}$ is defined by $\bar{\sigma} = (\uparrow, \downarrow)$ for $\sigma = (\downarrow, \uparrow)$. We note that the pair-hopping interaction in the Hamiltonian and the Fock terms are not taken into account. This is essential to reproduce the electronic states in the case of $t_A = t_B = 0$. The initial electronic wave function before the photoexcitation is obtained by solving the self-consistent equations. The photoirradiation is simulated by excitations of electrons from the highest

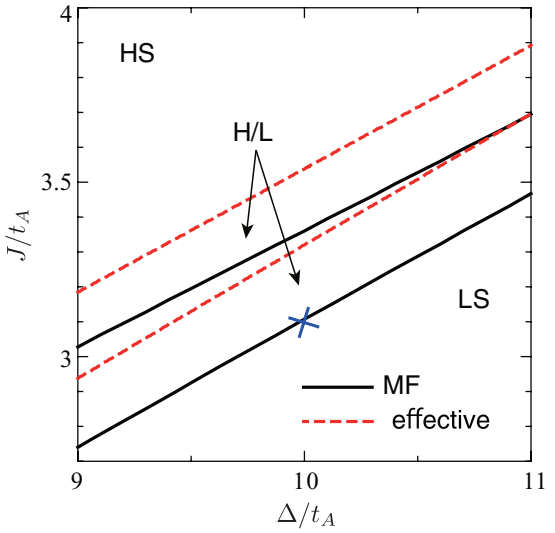

FIG. 11. (Color online) Phase diagram in the ground state obtained by the mean-field (MF) approximation. A two-dimensional $N = 10 \times 10$ site cluster with a periodic boundary condition is adopted. As a comparison, phase boundaries obtained by the exact-diagonalization method on the effective Hamiltonian ($N = 8$) are plotted by broken lines. The abbreviations HS, LS, and H/L represent the HS phase, the LS phase, and the HS-LS mixed phase, respectively. The parameters are chosen to be $U = 4J$, $U' = 2J$, and $t_B = 0.05t_A$.

occupied levels to the lowest unoccupied ones at time $\tau = 0$ where the z component of the total spin-angular momentum and the total momentum are conserved. The time evolution of the wave function is calculated in the time-dependent mean-field scheme. The time-dependent Schrödinger equation for the νth level, $|\phi_\nu(\tau)\rangle$, is given as

$$|\phi_\nu(\tau)\rangle = P \exp\left[-i \int_0^\tau d\tau' \mathcal{H}_{\rm MF}(\tau')\right] |\phi_\nu(0)\rangle\,, \qquad (30)$$

where $\mathcal{H}_{\rm MF}(\tau)$ is the time-dependent Hamiltonian given in Eq. (29), and P is the time-ordering operator. The wave function at time $\tau + d\tau$, where $d\tau$ is a short-time increment, is calculated from the wave function at time τ by expanding the exponential factor as

$$|\phi_\nu(\tau + d\tau)\rangle = \sum_\mu \langle\varphi_\mu(\tau)|\phi_\nu(\tau)\rangle e^{-i\varepsilon_\mu(\tau)d\tau} |\varphi_\mu(\tau)\rangle, \qquad (31)$$

where $|\varphi_\mu(\tau)\rangle$ is the eigenstate of $\mathcal{H}_{\rm MF}(\tau)$ with the eigenenergy $\varepsilon_\mu(\tau)$. In the numerical calculation, we take $d\tau t_A = 10^{-3} \sim 10^{-4}$, and check that the total energy is conserved within the order of 10^{-2} percent.

The phase diagram in the ground state is presented in Fig. 11. The phase boundaries are determined by the HS density. We also plot the results obtained by the exact-diagonalization method applied to the effective Hamiltonian shown in Fig. 4. The two results are qualitatively similar to each other, although the LS phase in the present calculation shifts to a low-J region.

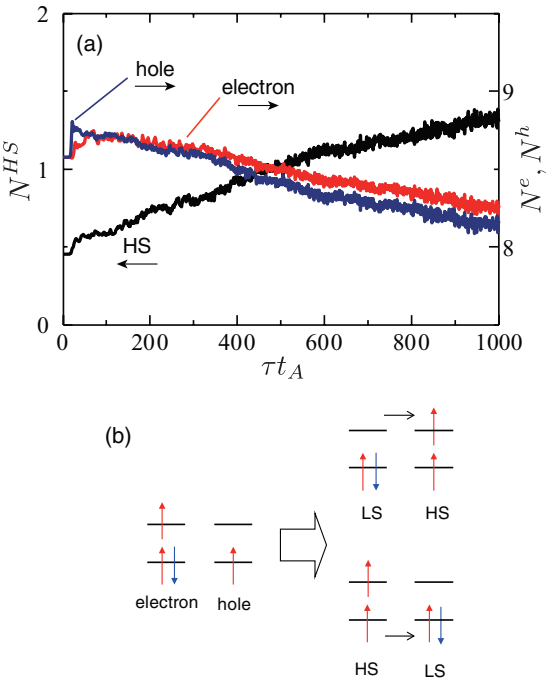

FIG. 12. (Color online) (a) Time evolutions of the numbers of the HS state, the electron state, and the hole state. (b) Schematic picture of the electron-hole pair annihilation processes. A two-dimensional $N = 10 \times 10$ site cluster with a periodic boundary condition is adopted. The parameters are chosen to be $U = 4J$, $U' = 2J$, $J = 3.1t_A$, $\Delta = 10t_A$, $t_B = 0.05t_A$, and $N_{ph} = 10$.

B. Numerical results

The time evolution of the photoexcited electronic state is examined in a two-dimensional $N = 10 \times 10$ site cluster with a periodic boundary condition. The number of photons in the cluster is chosen to be $N_{\rm ph} = 10$, which is introduced into the LS phase near the boundary at $J = 3.1t_A$, $\Delta = 10t_A$, which is indicated by a cross symbol in Fig. 11. We monitor the numbers of the HS state, the photodoped electron state, and the photodoped hole state by the following physical quantities, $N^{\rm HS} = \sum_{i\sigma} N^{\rm HS}_{i\sigma}$, $N^e = \sum_{i\sigma} N^e_{i\sigma}$, and $N^h = \sum_{i\sigma} N^h_{i\sigma}$ with

$$N^e_{i\sigma} = \langle n_{iA\sigma}\rangle (1 - \langle n_{iA\bar\sigma}\rangle) \langle n_{iB\sigma}\rangle \langle n_{iB\bar\sigma}\rangle\,, \qquad (32)$$

$$N^h_{i\sigma} = (1 - \langle n_{iA\sigma}\rangle)(1 - \langle n_{iA\bar\sigma}\rangle) \langle n_{iB\sigma}\rangle (1 - \langle n_{iB\bar\sigma}\rangle), \qquad (33)$$

and

$$N^{HS}_{i\sigma} = \langle n_{iA\sigma}\rangle (1 - \langle n_{iA\bar\sigma}\rangle) \langle n_{iB\sigma}\rangle (1 - \langle n_{iB\bar\sigma}\rangle), \qquad (34)$$

respectively. We note that these are defined as products of the mean-field number density in each orbital and spin, instead of the projection operators such as P^e_i [Eq. (24)], P^h_i [Eq. (25)], and P^H_i [Eq. (12)], which cannot be calculated directly in the mean-field scheme.

The time dependence of these numbers is plotted in Fig. 12(a). Except for time below $\tau t_A = 10$, where all three are almost constant, $N^{\rm HS}$ increases, and N^e and N^h decrease monotonically. That is, changes in the three numbers are correlated with each other. This result can be interpreted as indicating that the HS states are created by annihilation of the photoinduced electron and hole states. Let us consider a

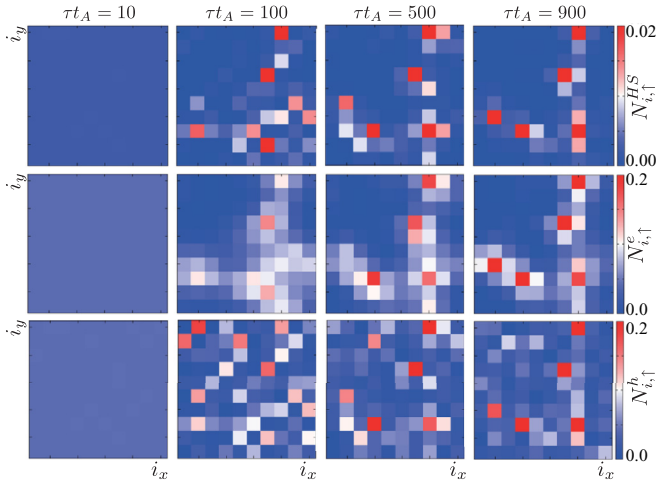

FIG. 13. (Color online) Snapshots of the electron state, the hole state, and the HS state. The time is chosen to be $10t_A^{-1}$, $100t_A^{-1}$, $500t_A^{-1}$, and $900t_A^{-1}$. A two-dimensional $N = 10 \times 10$ site cluster with a periodic boundary condition is adopted. The parameters are chosen to be $U = 4J$, $U' = 2J$, $J = 3.1t_A$, $\Delta = 10t_A$, $t_B = 0.05t_A$, and $N_{\rm ph} = 10$.

situation where the electron and hole states adjoin, as shown in Fig. 12(b). When an electron in the A orbital transfers to the hole state, a LS-HS pair is generated. This pair is also generated by the electron transfer in the B orbital. This is termed the electron-hole pair annihilation process. The HS-creation process is visualized in Fig. 13. At $\tau = 10t_A^{-1}$, the three numbers are almost homogeneous. At $\tau = 100t_A^{-1}$, the distributions for the electron states start to be inhomogeneous and a vertical shape domain appears, whereas the holes are still itinerant. After that, the electron states in the vertical-shape domain begin to be localized and the hole states are also localized simultaneously. The HS states are created at the sites where both $N^e_{i\uparrow}$ and $N^h_{i\uparrow}$ are large. After the HS states are generated, $N^h_{i\uparrow}$ and $N^e_{\uparrow}$ at the same sites still remain large. This observation does not contradict electron-hole annihilation, but rather is due to the definitions of $N^h_{i\uparrow}$ and $N^e_{i\uparrow}$ [see Eqs. (33) and (32)]; these are represented by the products of the mean-field number density, instead of the projection operators.

The electron-hole pair annihilation processes are also examined by the time-dependent density of states (DOS). We define the DOS as

$$A(\omega) = A^e(\omega) + A^h(\omega), \tag{35}$$

with the electron part

$$A^e(\omega) = \sum_\nu \delta[\omega - \varepsilon_\nu(\tau)]\langle c^\dagger_\nu c_\nu\rangle \tag{36}$$

and the hole part

$$A^h(\omega) = \sum_\nu \delta[\omega - \varepsilon_\nu(\tau)]\langle c_\nu c^\dagger_\nu\rangle. \tag{37}$$

The operator $c^\dagger_\nu$ is the creation operator obtained by diagonalizing the Hamiltonian at time τ, $\varepsilon_\nu(\tau)$ is the corresponding mean-field energy, and $\langle\cdots\rangle$ is the average in terms of the wave function of $|\psi(\tau)\rangle$. In the numerical calculation, the delta

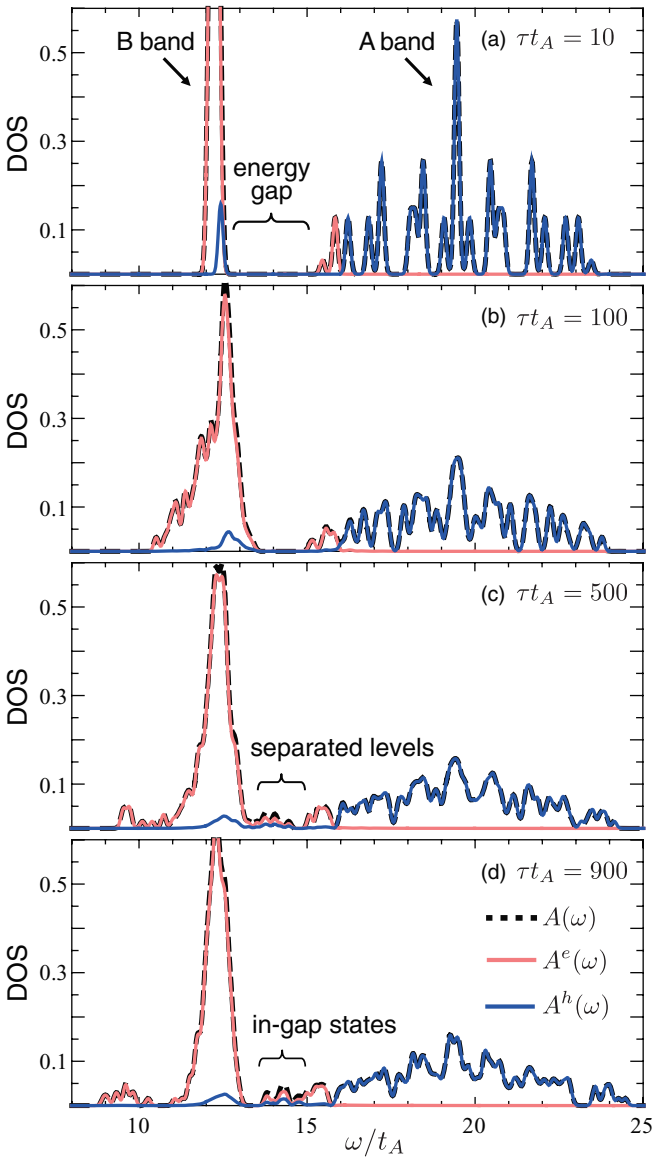

FIG. 14. (Color online) Density of states (DOS). The electron part and the hole part of the DOS are represented by pink solid and blue solid lines, respectively. The time is taken to be $10t_A^{-1}$, $100t_A^{-1}$, $500t_A^{-1}$, and $900t_A^{-1}$. A two-dimensional $N = 10 \times 10$ site cluster with a periodic boundary condition is adopted. The parameters are chosen to be $U = 4J$, $U' = 2J$, $J = 3.1t_A$, $\Delta = 10t_A$, $t_B = 0.05t_A$, $\eta = 0.1t_A$, and $N_{ph} = 10$.

functions in Eqs. (36) and (37) are replaced by the Lorentz function with a damping constant $\eta = 0.1t_A$.

The numerical results of the time-dependent DOS are shown in Fig. 14. At $\tau = 10t_A^{-1}$, an energy gap exists between the narrow B band and the wide A band. Tiny weights of the hole and electron parts of the DOS are observed at the top of the B band and the bottom of the A band, respectively. At time $\tau = 500t_A^{-1}$, the top of the B band and the bottom of the A band start to separate from the main bands. Finally, at $\tau = 900t_A^{-1}$, the original gap is almost filled by in-gap states originating from the localization of the electron and hole states.

Based on these results, we consider the energy balance in the electron-hole pair annihilation processes. The on-site

mean-field energies of the LS, HS, electron, and hole states are given by $E^{\rm LS}_{\rm MF} = U$, $E^{\rm HS}_{\rm MF} = U' + \Delta - J$, $E^{e}_{\rm MF} = U + 2U' + \Delta - J$, and $E^{h}_{\rm MF} = 0$, respectively. When one electron-hole pair is changed into one LS state and one HS state, the energy is changed as $\Delta E_{eh\to LH} \equiv (E^{\rm LS}_{\rm MF} + E^{\rm HS}_{\rm MF}) - (E^{e}_{\rm MF} + E^{h}_{\rm MF}) = -U'$ which is negative, i.e., an energy loss. This energy is compensated for by the kinetic energy of the hole and electron states, which are not related to the pair-annihilation processes. This is confirmed in the DOS at $\tau t_A = 900$ [see Fig. 14(d)]; the hole part of the DOS in the B-orbital band distributes not only to the top of the band, but also down to the middle of the band. This indicates an increasing of the kinetic energy of holes with time.

In the last part of this section, we examine, on the time-evolution of the photoinduced HS generation, roles of the relativistic spin-orbit (SO) interaction which breaks the spin angular-momentum conservation. Here we mimic the SO interaction in the $3d$ orbitals as follows:

$$\mathcal{H}_{\rm SO} = i\xi \sum_i (c^\dagger_{ia\uparrow} c_{ib\downarrow} + c^\dagger_{ia\downarrow} c_{ib\uparrow} - c^\dagger_{ib\uparrow} c_{ia\downarrow} - c^\dagger_{ib\downarrow} c_{ia\uparrow}), \tag{38}$$

with the SO interaction constant ξ. It is demonstrated that when this interaction acts on the LS state, the HS state is created as follows:

$$\mathcal{H}_{\rm SO} c^\dagger_{ib\uparrow} c^\dagger_{ib\downarrow} |0\rangle = -i\xi (c^\dagger_{ia\uparrow} c^\dagger_{ib\uparrow} - c^\dagger_{ia\downarrow} c^\dagger_{ib\downarrow})|0\rangle. \tag{39}$$

Numerical results of the time evolutions of $N^{\rm HS}$ and N^h are presented in Fig. 15, where the SO interaction constant is taken to be $\xi = 0$ and $0.3t_A$. Before $\tau = 200t_A^{-1}$, the SO interaction effects are not seen in $N^{\rm HS}$. However, beyond $\tau = 200t_A^{-1}$, $N^{\rm HS}$ starts to decrease in the case of a finite ξ. The observed reduction of the HS state in the case of finite ξ is due to the transition from the HS to LS states through the SO interaction, as shown schematically in Fig. 15(b). This result indicates that effect of the SO interaction on the spin-state transition is destructive rather than constructive.

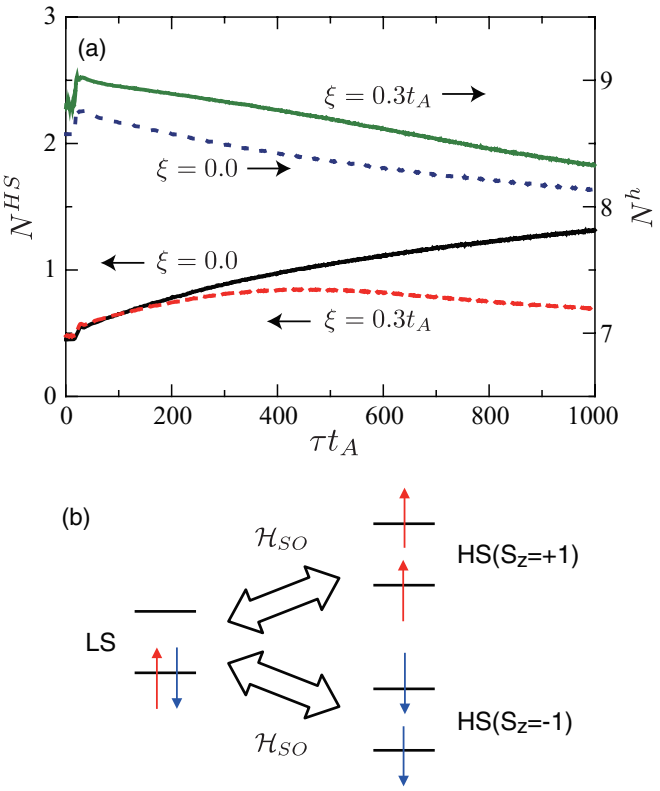

FIG. 15. (Color online) (a) The numbers of the HS state and the hole state in the model with the spin-orbit (SO) interaction. A two-dimensional $N = 10 \times 10$ site cluster with a periodic boundary condition is adopted. The parameters are chosen to be $U = 4J$, $U' = 2J$, $J = 3.1t_A$, $\Delta = 10t_A$, $t_B = 0.05t_A$, and $N_{ph} = 10$. Ten data sets with different initial values for the time evolutions are averaged. (b) Schematic picture of the transition between the HS state and the LS state due to the SO interaction.

V. DISCUSSION AND CONCLUSION

In this section, we remark on (i) the connection between the calculated results in the photoexcited metastable state and the time-dependent simulation in the photoexcited state, which are presented in Secs. III and IV, respectively, and (ii) the implications of the present theoretical results for recent experiments.

In Sec. IV, we show in the time-dependent simulation that a pair annihilation of photodoped electron and hole generates an HS state. In this scheme, we consider the stability of the HS state and the role of the photodoped hole. The correlation between the local HS state and the hole state around the local HS state is examined numerically. We focus on the relationship between the number density of the local HS state at time τ, $N^{\rm HS}_{i\sigma}(\tau)$, and that of the hole state around the site i at time τ' denoted as $\rho_{i\sigma}(\tau') \equiv \sum'_j N^h_{j\sigma}(\tau')$, where $\sum'_j$ is a summation for the NN sites of i. Data sets of $\rho_{i\sigma}(\tau)$ and $N^{\rm HS}_{i\sigma}(\tau + \Delta\tau)$ with $\Delta\tau = 10t_A^{-1}$ are obtained in 100 times simulations with different initial states. Figure 16 shows a positive correlation between them. In particular, in the region of high hole density, $\rho_{i\sigma}(\tau) \gtrsim 0.1$, there are little data for small $N^{\rm HS}_{i\sigma}(\tau + \Delta\tau)$. On the other hand, in the region of low hole density, $\rho_{i\sigma}(\tau) \lesssim 0.1$, the value of $N^{\rm HS}_{i\sigma}(\tau + \Delta\tau)$ distributes. These results are interpreted as indicating that in the case where the hole density around the photoinduced HS state is low, the probability of the survival of the HS state number is randomly distributed. On the other hand, the HS states surrounded by many holes have a long lifetime. These relations between the photodoped hole and the HS state are consistent with the results in Sec. III, where the HS state is stabilized by forming the HS-hole bound state.

Next we compare the present calculated results with the experimental data reported in Ref. 34. As introduced previously, the key points in the optical pump-probe experiments in $R{\rm BaCo_2O_{6-\delta}}$ are (a) a photoinduced metallic state that is different from the high-temperature metallic state, and (b) that this photoinduced state strongly depends on the R species. From the calculated results, we propose that the observed metallic state can be attributed to the HS-hole bound state. We note that since the HS-hole bound state is a local object, the present results obtained in small clusters are considered to be applicable to cobalt oxides. The experimental spectral weight induced by the photon pumping is interpreted to be the dipole transition in the bound state. We have checked using

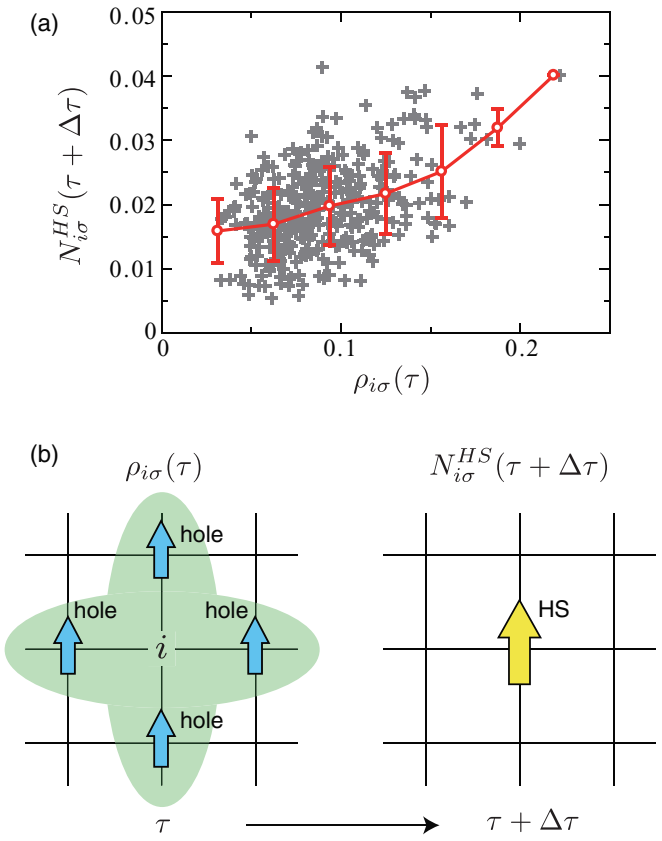

FIG. 16. (Color online) Correlation between the number density of the local HS state at time $\tau + \Delta\tau$, $N_{i\sigma}^{HS}(\tau + \Delta\tau)$, and the number density of the hole state around the site i at time τ, $\rho_{i\sigma}(\tau)$. We take $\Delta\tau = 10/t_A$. A two-dimensional $N = 10 \times 10$ site cluster with the periodic boundary condition is adopted. The parameters are chosen to be $U = 4J$, $U' = 2J$, $J = 3.1t_A$, $\Delta = 10t_A$, $t_B = 0.05t_A$, $N_{ph} = 10$, and $\Delta\tau = 10t_A^{-1}$.

the exact-diagonalization method for a small-size cluster that a clear bound state between thermal hole carriers and the HS states is not stabilized at finite temperatures.[36] It is well known that in perovskite crystal, the electron transfer intensity is systematically controlled by the R species through a changing of the Co-O-Co bond angle. The smaller the ionic radius of the R ion, the smaller the e_g bandwidth. With increasing ionic radius from Tb to Sm, the photoinduced metallic state is increasingly evident in experimental optical conductivity spectra. These data correspond to the calculated results in the phase diagram in Fig. 4. The increasing of the transfer integral of the A band, equivalent to the decrease of Δ/t_A, is indicated by the arrow in this phase diagram. The system is transferred from the phase, where the spin-state is not changed by photoexcitation, to the phase, where the HS state is induced by photoirradiation. This consistency between the theory and the experiments is further evidence of the existence of the photoinduced HS-hole bound state.

Finally, we briefly discuss the relation between the present photoinduced HS-hole bound state and the phase separation in cobaltites induced by chemical carrier doping. A number of experiments have suggested spatial segregation of the hole-rich FM metallic and hole-poor insulating regions in lightly hole doped $La_{1-x}Sr_xCoO_3$. This is believed to be the origin of observed giant magnetoresistance phenomena. Theoretical calculations have shown that an inhomogeneous electronic structure is unstable against a phase separation of the HS FM and LS insulating phases.[33,40,41] As well as the present finding of the photoinduced HS-hole bound state, the phase segregation induced by chemical doping is attributed to the energy balance where the crystal-field energy and the magnetic and kinetic energies due to the double exchange interactions are fully gained in the LS insulating phase and the HS metallic phase, respectively, in comparison with the homogeneous mixed spin-state phase. We found in our previous work[33] that the bandwidth in the B band is essential to stabilize the chemically induced phase separation. This tendency is similar to the present results shown in Fig. 8 where the photoinduced bound state is realized in the region of small t_B. In contrast, there is a discrepancy between the two results, i.e., a macroscopic scale of the phase separation and the local bound state. Further investigations will be required to reveal detailed connection between the two phenomena.

In conclusion, we have studied the photoinduced spin-state change in a correlated electron system. The photoinduced metastable state was examined in the effective Hamiltonian which is derived by the two-orbital Hubbard model. By photoirradiation into the LS phase near the phase boundary with a mixed phase, the HS state is induced and is stabilized by forming a bound state with a photodoped hole state. An optical transition inside this bound state appears. A time-dependent simulation of the photoexcited state was also performed on the two-orbital Hubbard model in the time-dependent mean-field scheme. A pair annihilation of the photodoped electron and hole states generates the HS state. This process is reflected in the time-dependent DOS. The present results propose a new state of photoexcited matter in correlated electron system with multiple degrees of freedom.

ACKNOWLEDGMENTS

The authors would like to thank H. Matsueda, Y. Inoue, Y. Okimoto, S. Koshihara, S. Iwai, and T. Arima for valuable discussions. This work was supported by KAKENHI from MEXT, Optical Science of Dynamically Correlated Electrons (DYCE), Tohoku University "Evolution" program, and Grand Challenges in Next-Generation Integrated Nanoscience. Y.K. is supported by the global COE program "Weaving Science Web beyond Particle-Matter Hierarchy" of MEXT, Japan. Parts of the numerical calculations were performed on the supercomputing systems in ISSP, University of Tokyo, and Kyoto University.

APPENDIX A: EXCHANGE CONSTANTS IN EFFECTIVE HAMILTONIAN FOR THE INITIAL STATE

In this appendix, explicit formulas of the exchange constants in the effective Hamiltonian for the initial state, given in Eq. (10), are presented. These are represented by the energy parameters in the original two-orbital Hubbard model as

$$J_{HH} = \frac{t_A^2 + t_B^2}{U + J}, \tag{A1}$$

$$J_{LL} = \frac{4 f_B^2 f_A^2 \left(t_A^2 + t_B^2\right)}{2U' + 2\Delta_J - U - J}, \tag{A2}$$

$$J_{HL} = (t_A^2 + t_B^2)\left(\frac{f_B^2}{U' + \Delta_J - \Delta} + \frac{f_A^2}{U' + \Delta_J + \Delta}\right), \tag{A3}$$

$$J_{++} = 2t_A t_B f_B f_A \left(\frac{1}{U + J} + \frac{1}{2U' - U - J + 2\Delta_J}\right), \tag{A4}$$

$$J_{+-} = 2t_A t_B \left(\frac{f_B^2}{U' + \Delta_J - \Delta} + \frac{f_A^2}{U' + \Delta_J + \Delta}\right), \tag{A5}$$

where we define $\Delta_J = \sqrt{\Delta^2 + J^2}$.

APPENDIX B: EFFECTIVE HAMILTONIAN FOR THE PHOTOEXCITED METASTABLE STATE

In this appendix, explicit formulas of the effective Hamiltonian for the photoinduced metastable state are presented. Matrix elements in terms of the electronic states in NN sites are shown. These are classified by the electron number n and the z component of the total spin-angular momentum S_z as $\mathcal{H}^{(n,S_z)}$. The wave functions in the two sites are denoted as $|\psi_i, \psi_j\rangle$. In the following notation, each term in the Hamiltonian in Eq. (17) is given as $\mathcal{H}_{eh} = \mathcal{H}^{(4,0)} + \mathcal{H}^{(4,1)}$, $\mathcal{H}_e = \mathcal{H}^{(5,3/2)} + \mathcal{H}^{(5,1/2)}$, and $\mathcal{H}_h = \mathcal{H}^{(3,3/2)} + \mathcal{H}^{(3,1/2)}$.

(1) ($n = 3$, $S_z = 3/2$)

$$\mathcal{H}^{(3,3/2)} = \begin{pmatrix} 0 & t_A \\ t_A & 0 \end{pmatrix}. \tag{B1}$$

The basis set is $\{|\psi_{h\uparrow}, \psi_{H+1}\rangle\, |\psi_{H+1}, \psi_{H\uparrow}\rangle\}$.

(2) ($n = 3$, $S_z = 1/2$)

$$\mathcal{H}^{(3,1/2)} = \begin{pmatrix} -J_{hH} & \frac{J_{hH}}{\sqrt{2}} & 0 & \frac{t_A}{\sqrt{2}} & 0 & 0 \\ \sqrt{2}J_{hH} & -\frac{J_{hH}}{2} & \frac{t_A}{\sqrt{2}} & \frac{t_A}{2} & 0 & 0 \\ 0 & \frac{t_A}{\sqrt{2}} & -J_{hH} & \frac{J_{hH}}{\sqrt{2}} & 0 & 0 \\ \frac{t_A}{\sqrt{2}} & \frac{t_A}{2} & \sqrt{2}J_{hH} & -\frac{J_{hH}}{2} & 0 & 0 \\ 0 & 0 & 0 & 0 & -J_{hL} & f_B^2 t_B \\ 0 & 0 & 0 & 0 & f_B^2 t_B & -J_{hL} \end{pmatrix}, \tag{B2}$$

where

$$J_{hH} = \frac{t_A^2}{4J} + \frac{t_B^2}{U + U'} + \frac{t_B^2 f_B^2}{\Delta + J + U - U' - \Delta_J} + \frac{t_B^2 g_B^2}{\Delta + J + U - U' + \Delta_J}, \tag{B3}$$

$$J_{hL} = \frac{t_B^2 f_B^2 g_B^2}{2\Delta_J} + \frac{t_B^2 f_A^2}{\Delta + 2U' - J + \Delta_J} + \frac{3 f_A^2 t_A^2}{2} \frac{1}{\Delta - U + U' + \Delta_J - J} + \frac{3 f_A^2 t_A^2}{2} \frac{1}{\Delta - U + U' + \Delta_J + J}, \tag{B4}$$

with

$$g_B = \left[1 + \left(\frac{\Delta}{I} + \sqrt{1 + \frac{\Delta^2}{I^2}}\right)^2\right]^{-1/2}. \tag{B5}$$

The basis set is $\{|\psi_{h\downarrow}, \psi_{H+1}\rangle, |\psi_{h\uparrow}, \psi_{H0}\rangle, |\psi_{H+1}, \psi_{h\downarrow}\rangle, |\psi_{H0}, \psi_{h\uparrow}\rangle, |\psi_{h\uparrow}, \psi_L\rangle, |\psi_L, \psi_{h\uparrow}\rangle\}$.

(3) ($n = 4$, $S_z = 1$)

$$\mathcal{H}^{(4,1)} = \begin{pmatrix} J_{eh1} & \alpha_{eh} J_{eh1} \\ \alpha_{eh} J_{eh1} & J_{eh1} \end{pmatrix}, \tag{B6}$$

where

$$J_{eh1} = (t_A^2 + t_B^2)\left(\frac{f_B^2}{U' - \Delta + \Delta_J} + \frac{g_B^2}{U' - \Delta - \Delta_J}\right), \tag{B7}$$

and

$$\alpha_{eh} = \frac{2t_A t_B}{t_A^2 + t_B^2}. \tag{B8}$$

The basis set is $\{|\psi_{e\uparrow}, \psi_{h\uparrow}\rangle |\psi_{h\uparrow}, \psi_{e\uparrow}\rangle\}$.

(4) ($n = 4$, $S_z = 0$)

$$\mathcal{H}^{(4,0)} = \frac{1}{2}\begin{pmatrix} J_{eh+} & J_{eh-} & 0 & 0 \\ J_{eh-} & J_{eh+} & 0 & 0 \\ 0 & 0 & J_{eh+} & J_{eh-} \\ 0 & 0 & J_{eh-} & J_{eh+} \end{pmatrix} + \frac{\alpha_{eh}}{2}\begin{pmatrix} 0 & 0 & J_{eh+} & J_{eh-} \\ 0 & 0 & J_{eh-} & J_{eh+} \\ J_{eh+} & J_{eh-} & 0 & 0 \\ J_{eh-} & J_{eh+} & 0 & 0 \end{pmatrix}, \tag{B9}$$

where $J_{eh\pm} = J_{eh1} \pm J_{eh2}$ and

$$J_{eh2} = \left(t_A^2 + t_B^2\right)\left(\frac{f_B^2}{U' - \Delta + \Delta_J - 2J} + \frac{g_B^2}{U' - \Delta - \Delta_J - 2J}\right). \tag{B10}$$

The basis set is $\{|\psi_{e\downarrow}, \psi_{h\uparrow}\rangle, |\psi_{e\uparrow}, \psi_{h\downarrow}\rangle, |\psi_{h\uparrow}, \psi_{e\downarrow}\rangle, |\psi_{h\downarrow}, \psi_{e\uparrow}\rangle\}$.

(5) ($n = 5$, $S_z = 3/2$)

$$\mathcal{H}^{(5,3/2)} = \begin{pmatrix} 0 & t_B \\ t_B & 0 \end{pmatrix}. \tag{B11}$$

The basis set is $\{|\psi_{e\uparrow}, \psi_{H+1}\rangle, |\psi_{H+1}, \psi_{e\uparrow}\rangle\}$.

(6) ($n = 5$, $S_z = 1/2$)

$$\mathcal{H}^{(5,1/2)} = \begin{pmatrix} -J_{eH} & \frac{J_{eH}}{\sqrt{2}} & 0 & -\frac{t_B}{\sqrt{2}} & 0 & 0 \\ J_{eH}\sqrt{2} & -\frac{J_{eH}}{2} & -\frac{t_B}{\sqrt{2}} & -\frac{t_B}{2} & 0 & 0 \\ 0 & -\frac{t_B}{\sqrt{2}} & -J_{eH} & \frac{J_{eH}}{\sqrt{2}} & 0 & 0 \\ -\frac{t_B}{\sqrt{2}} & -\frac{t_B}{2} & J_{eH}\sqrt{2} & -\frac{J_{eH}}{2} & 0 & 0 \\ 0 & 0 & 0 & 0 & -J_{eL} & -f_B^2 t_A \\ 0 & 0 & 0 & 0 & -f_B^2 t_A & -J_{eL} \end{pmatrix}, \tag{B12}$$

where

$$J_{eH} = \frac{t_B^2}{4J} + \frac{t_A^2}{U+U'+2J} + \frac{t_A^2 f_B^2}{\Delta+U-U'+J-\Delta_J} + \frac{t_A^2 g_B^2}{\Delta+U-U'+J+\Delta_J}, \quad \text{(B13)}$$

and

$$J_{eL} = \frac{t_A^2 f_B^2 g_B^2}{2\Delta_J} + \frac{t_A^2 f_A^2}{\Delta+2U'+J+\Delta_J} + \frac{f_A^2 t_B^2}{2}\frac{3}{\Delta-U+U'+\Delta_J-J} + \frac{f_A^2 t_B^2}{2}\frac{1}{\Delta-U+U'+\Delta_J+J}. \quad \text{(B14)}$$

The basis set is $\{|\psi_{e\downarrow},\psi_{H+1}\rangle,|\psi_{e\uparrow},\psi_0\rangle,|\psi_{H+1},\psi_{e\downarrow}\rangle,|\psi_{H0},\psi_{e\uparrow}\rangle,|\psi_{e\uparrow},\psi_L\rangle,|\psi_L,\psi_{e\uparrow}\rangle\}$.

APPENDIX C: HARD-CORE TWO-FERMION MODEL

In this appendix, we introduce the hard-core two-fermion model. As shown in Sec. III C, this model well reproduces the optical absorption spectra in the photoinduced metastable state, when the HS-hole bound state is not induced. The hard-core two-fermion model is defined by

$$\mathcal{H}_{\rm HC} = -t_A \sum_{\langle ij\rangle}(a_i^\dagger a_j + \text{H.c.}) - t_B \sum_{\langle ij\rangle}(b_i^\dagger b_j + \text{H.c.}) - t_{ex} \sum_{\langle ij\rangle}(a_i^\dagger b_j^\dagger b_i a_j + \text{H.c.}), \quad \text{(C1)}$$

where a_i and b_i are the spin-less fermion operators at site i and describe annihilations of the electron state and the hole state, respectively. We take a condition of $a_i^\dagger b_i^\dagger = 0$. The first and second terms represent kinetic motions of the electron and hole states in the LS phase, respectively, and the third term represents an exchange of the electron and hole states.

This model is derived in the limiting case of $\Delta \gg I$ in the original Hamiltonian as follows. From Eqs. (4)–(6), we have $|\psi_L\rangle = c_{B\uparrow}^\dagger c_{B\downarrow}^\dagger|0\rangle$ which is set to be a vacuum, $|\tilde{0}\rangle$, in this model. The electron and hole states are defined from this vacuum as $|\tilde{e}\rangle = a_i^\dagger|\tilde{0}\rangle$ and $|\tilde{h}\rangle = b_i^\dagger|\tilde{0}\rangle$, respectively. The matrix elements for the exchange of the electron (hole) and LS states, corresponding to the first (second) term in Eq. (C1), are given by $t_A f_B^2 \sim t_A$ ($t_B f_B^2 \sim t_B$) from Eqs. (B2) and (B12). The exchange of the electron and hole states, corresponding to the last term in Eq. (C1), are given in the matrix elements in Eqs. (B6) and (B9). We confirm numerically that this contribution to the optical spectra is much smaller than other terms, and set to be a small constant $t_{ex} = 10^{-10}t_A$ in the numerical calculation. In this effective model, the current operator along an α direction is given by

$$j_{\rm HC}^\alpha = it_A \sum_i (a_i^\dagger a_{i+\alpha} - \text{H.c.}) - it_B \sum_i (b_i^\dagger b_{i+\alpha} - \text{H.c.}). \quad \text{(C2)}$$

*Present address: Department of Physics, Hokkaido University, Sapporo 060-0810, Japan.

[1] S. Maekawa, T. Tohyama, S. E. Barnes, S. Ishihara, W. Koshibae, and G. Khliullin, *Physics of Transition Metal Oxides* (Springer Verlag, Berlin, 2004).

[2] K. Nasu, *Photo Induced Phase Transition* (World Scientific, Singapore, 2004), and references therein.

[3] M. Fiebig, K. Miyano, Y. Tomioka, and Y. Tokura, Science **280**, 1925 (1998).

[4] A. Cavalleri, Cs. Tóth, C. W. Siders, J. A. Squier, F. Ráksi, P. Forget, and J. C. Kieffer, Phys. Rev. Lett. **87**, 237401 (2001).

[5] H. Okamoto, T. Miyagoe, K. Kobayashi, H. Uemura, H. Nishioka, H. Matsuzaki, A. Sawa, and Y. Tokura, Phys. Rev. B **83**, 125102 (2011).

[6] H. Matsueda and S. Ishihara, J. Phys. Soc. Jpn. **76**, 083703 (2007).

[7] Y. Kanamori, H. Matsueda and S. Ishihara, Phys. Rev. Lett. **103**, 267401 (2009); Phys. Rev. B **82**, 115101 (2010).

[8] S. Iwai, S. Tanaka, K. Fujinuma, H. Kishida, H. Okamoto, and Y. Tokura, Phys. Rev. Lett. **88**, 057402 (2002).

[9] M. Chollet, L. Guerin, N. Uchida, S. Fukaya, H. Shimoda, T. Ishikawa, K. Matsuda, T. Hasegawa, A. Ota, H. Yamochi, G. Saito, R. Tazaki, S. Adachi, and S. Koshihara, Science **307**, 86 (2005).

[10] N. Tajima, J. Fujisawa, N. Naka, T. Ishihara, R. Kato, Y. Nishio, and K. Kajita, J. Phys. Soc. Jpn. **74**, 511 (2005).

[11] K. Yonemitsu and K. Nasu, J. Phys. Soc. Jpn. **75**, 011008 (2006).

[12] O. Sato, T. Iyoda, A. Fukushima, and K. Hashimoto, Science **272**, 704 (1996).

[13] A. Bleuzen, C. Lomenech, V. Escax, F. Villain, F. Varret, C. C. dit Moulin, and M. Verdaguer, J. Am. Chem. Soc. **122**, 6648 (2000).

[14] V. Escax, A. Bleuzen, C. C. dit Moulin, F. Villain, A. Goujon, F. Varret, and M. Verdaguer, J. Am. Chem. Soc. **123**, 12536 (2001).

[15] O. Sato, J. Photochem. Photobio. C: Photochem. Rev. **5**, 203 (2004).

[16] N. Willenbacher and H. Spiering, J. Phys. C **21**, 1423 (1988).

[17] A. L. Tchougréeff and M. B. Darkhovskii, Int. J. Quantum Chem. **57**, 903 (1996).

[18] M. Nishino, K. Boukheddaden, Y. Konishi, and S. Miyashita, Phys. Rev. Lett. **98**, 247203 (2007).

[19] S. Miyashita, P. A. Rikvold, T. Mori, Y. Konishi, M. Nishino, and H. Tokoro, Phys. Rev. B **80**, 064414 (2009).

[20] C. Frontera, J. L. García-Muñoz, A. Llobet, and M. A. G. Aranda, Phys. Rev. B **65**, 180405(R) (2002).

[21] S. Tsubouchi, T. Kyomen, M. Itoh, P. Ganguly, M. Oguni, Y. Shimojo, Y. Morii, and Y. Ishii, Phys. Rev. B **66**, 052418 (2002).

[22] Y. Okimoto, X. Peng, M. Tamura, T. Morita, K. Onda, T. Ishikawa, S. Koshihara, N. Todoroki, T. Kyomen, and M. Itoh, Phys. Rev. Lett. **103**, 027402 (2009).

[23] K. Asai, P. Gehring, H. Chou, and G. Shirane, Phys. Rev. B **40**, 10982 (1989).

[24]Y. Tokura, Y. Okimoto, S. Yamaguchi, H. Taniguchi, T. Kimura, and H. Takagi, Phys. Rev. B **58**, 1699(R) (1998).
[25]R. R. Heikes, R. C. Miller, and R. Mazelsky, Physica **30**, 1600 (1964).
[26]P. M. Raccah and J. B. Goodenough, Phys. Rev. **155**, 932 (1967).
[27]S. Yamaguchi, Y. Okimoto, and Y. Tokura, Phys. Rev. B **54**, 11022(R) (1996).
[28]T. Saitoh, T. Mizokawa, A. Fujimori, M. Abbate, Y. Takeda, and M. Takano, Phys. Rev. B **55**, 4257 (1997).
[29]C. N. R. Rao, Om Parkash, D. Bahadur, P. Ganguly, and S. Nagabhushana, J. Solid State Chem. **22**, 353 (1977).
[30]M. A. Señarís-Rodríguez and J. B. Goodenough, J. Solid State Chem. **118**, 323 (1995).
[31]M. Itoh and I. Natori, J. Phys. Soc. Jpn. **64**, 970 (1995).
[32]K. Tsutsui, J. Inoue, and S. Maekawa, Phys. Rev. B **59**, 4549 (1999).
[33]R. Suzuki, T. Watanabe, and S. Ishihara, Phys. Rev. B **80**, 054410 (2009).
[34]Y. Okimoto, T. Miyata, M. S. Endo, M. Kurashima, K. Onda, T. Ishikawa, S. Koshihara, M. Lorenc, E. Collet, H. Cailleau, and T. Arima, Phys. Rev. B **84**, 121102(R) (2011).
[35]S. Iwai, S. Tomimoto, Y. Okimoto, J. P. He, Y. Kaneko, H. Okamoto, and Y. Tokura, Meeting abstracts of the Physical Society of Japan, **59**(2-4), 673, 13pPSA-75 (2004).
[36]Y. Kanamori, H. Matsueda, and S. Ishihara, Phys. Rev. Lett. **107**, 167403 (2011).
[37]D. L. Khomskii and U. Löw, Phys. Rev. B **69**, 184401 (2004).
[38]A. D. McLachlan and M. A. Ball, Rev. Mod. Phys. **36**, 844 (1964).
[39]A. Terai and Y. Ono, Prog. Theor. Phys. Suppl. **113**, 177 (1993).
[40]E. L. Nagaev, Phys. Status Solidi B **186**, 9 (1994).
[41]A. O. Sboychakov, K. I. Kugel, A. L. Rakhmanov, and D. I. Khomskii, Phys. Rev. B **80**, 024423 (2009).